JP Journal of Heat and Mass Transfer

https://pphmjopenaccess.com
https://doi.org/10.17654/0973576325043
Volume 38, Number 6, December 2025, Pages 811-833
P-ISSN: 0973-5763
E-ISSN: 3049-2556

GEOMETRICAL VARIATION FOR EVALUATION OF SOLAR CHIMNEY THERMAL PERFORMANCE

Tapas Kumar Panda[1], Ipsita Mishra[2], Mukundjee Pandey[1,*], Ardhendu Mouli Mohanty[1] and Madhusudan Pandey[3]

[1]Department of Mechanical Engineering
Centurion University of Technology and Management
Odisha - 752050, India

[2]School of Maritime Studies
Centurion University of Technology and Management
Odisha - 752050, India

[3]Department of Mechanical Engineering
Birsa Institute of Technology
Sindri, Dhanbad - 828123, India

Abstract

This study investigates the performance and optimization of solar chimneys by analysing the effects of varying key dimensions—

Received: June 18, 2025; Revised: October 6, 2025; Accepted: October 31, 2025
Keywords and phrases: solar chimney, collector radius, chimney height, vacuum pressure, air velocity, design optimization.
*Corresponding author
Communicated by Ch. Ramreddy

How to cite this article: Tapas Kumar Panda, Ipsita Mishra, Mukundjee Pandey, Ardhendu Mouli Mohanty and Madhusudan Pandey, Geometrical variation for evaluation of solar chimney thermal performance, JP Journal of Heat and Mass Transfer 38(6) (2025), 811-833.
https://doi.org/10.17654/0973576325043

Published Online: December 11, 2025

collector radius, collector height, chimney height, chimney radius, base and top radii, and chimney angle—on state variables (velocity, temperature, and pressure) at the chimney inlet. This study examines the function and the optimization of solar chimneys by research in the impact of variations in the number of key dimensions—specifically collector radius, collector height, chimney height, chimney radius, base and top radii, and chimney angle—on state parameters, including velocity, temperature, and pressure at the chimney inlet. Increasing the collector radius from 98 m to 122 m results in a rise in air velocity from 21.7 m/s to 25.6 m/s, vacuum pressure from -261 Pa to -326 Pa, and temperature from 54.2°C to 59.9°C, due to improved heat transfer. In contrast, increasing collector height from 1.8 m to 9.2 m leads to a decrease in velocity from 26.6 m/s to 22.3 m/s, temperature from 56.7°C to 48.7°C, and vacuum pressure from -355 Pa to -233 Pa. For the chimney, increasing height from 115 m to 255 m raises velocity from 21.7 m/s to 27.8 m/s and vacuum pressure from -218 Pa to -374 Pa, while reducing temperature from 57.3°C to 52°C. Increasing the chimney radius from 3.5 m to 11 m reduces velocity from 30.2 m/s to 18 m/s, temperature from 84.8°C to 54.2°C, and pressure from -440 Pa to -158 Pa. Additionally, adjusting the base and top radii, and chimney angle significantly impacts the system's performance, indicating the importance of optimization for maximum efficiency.

1. Introduction

A solar chimney is an efficient renewable energy device that uses sunlight to generate airflow and drive power using natural convection. Previous studies have proved that the efficiency of the system can be enhanced by changing the chimney height, collector area, and divergence angle. This article summarizes current studies on solar chimney systems with emphasis on the ability of solar chimney systems to improve natural ventilation, thermal comfort, and clean power production. Setayesh et al. investigated the effect of geometric parameters on the power production of solar chimneys through 49 various configurations in ANSYS-CFX, the result being that increasing the collector radius enhanced airflow velocity and increased power production by as much as 50%, and taller chimneys had a consistently near 30% increase in performance. Their simulations also

showed that the chimney diameter had a negligible effect, with a 6-10 collector-to-chimney height ratio giving optimal power [1]. Wang et al. explored the influence of geometry modifications in roof solar chimneys on thermal and ventilation performance and concluded that the upward velocities of flow were lower, and ventilation rates were higher by up to 25% under conditions as the width and gap of the cavity increased. The study shows that the thermal efficiency was reduced to about 15% by increasing the cross-sectional area of the channel; however, a reduced area ratio $(AR \leq 0.25)$ supported more uniform improvements in airflow and system sensitivity to buoyancy forces [2]. Cuce et al. investigated the influence of collector and chimney slope on power generation of a solar chimney power plant through 3D CFD modeling. They reported that a collector slope of 0.6° and a chimney divergence of 1.5° improved power from 46 kW to more than 216 kW at optimal geometry. A taller chimney provided decreasing returns, but a larger collector radius enhanced long-term efficiency [3]. Saleh et al. criticized solar chimney power plants, perceiving that phase change material and thermal storage improved efficiency by 40%. They also suggested that application of solar chimneys with external heat sources or new designs would boost production by over 50%, indicating vast potential for future growth [4]. Khayyaminejad et al. investigated the application of twisted tapes in an Earth Air Heat Exchanger in a solar chimney system and discovered the amendment enhanced heat exchange performance by 153% and minimized pipe length to be required up to 35 meters while preserving ventilation rates greater than 4.8 air changes per hour. Simulation determined the optimal performance in solar chimney diameter, twisted tape width ratio, and rotation rate as 1.25 m, 0.6, and 1.25, respectively, and most notably in hot, dry conditions [5]. Aziz and Elsayed investigated the impact of structural variations on the performance of solar chimney systems through numerical simulation and concluded that an increase in the chimney angle to 3° raised the maximum velocity by 200% and power output significantly. They also observed that the collector height was raised to 70% of the turbine radius and airflow mass flow was raised, but energy losses due to internal eddies were reduced by a concave chimney shape [6]. Singh and Kumar maximized a solar chimney power plant design with a 2° diverging angle of the chimney,

which boosted air speed by 59% and power by 290% over a reference design. Additional optimization with arc and fillet radii at the chimney base maximized maximum available power by 770% and mass flow rate by 154% over the reference design [7]. Tork et al. established that a geothermal and solar chimney system with a well of 200 meters would produce 15 kW, which would rise to 20 kW with a spacing of 1.5 km. Based on their research, a six-inlet system is 26% more efficient than a single well and can hence be used for a reliable supply of power in low solar radiation [8]. Ardila et al. experimented on the operation of a solar chimney for natural ventilation and thermal comfort for a residence in northeast Colombia and concluded that a 4-m, 55°-slope chimney was sufficient for thermal comfort in a 27 m^3 room for most months of the year according to ASHRAE Standard 55. The system operated best during January, March, April, August, November, and December, with September being the most extreme month for cooling [9]. Gong et al. investigated flowrate distribution in high solar chimneys and found that in traditional designs, there was up to 300% more airflow in lower floors than in higher floors, leading to extreme unevenness. They suggested a square-root-law (SRL) shape type of chimney design, which lowered the disparity in flowrate from 20 stories from 330.6% to just 15%, being an effective measure to enhance ventilation uniformity in tall buildings [10]. Bagheri and Hassanabad proposed a solar chimney power plant for city buildings. Their CFD simulation and experiment indicated that a vertical collector is able to generate four times the power of traditional systems with the same building area and chimney height. The best model, which was verified with Energy Plus and ANSYS Fluent, showed that higher chimneys have greater airflow velocity and all designs have an optimal diameter of the chimney for optimal performance [11]. Torabi et al. employed computational fluid dynamics (CFD) to investigate the effect of geometry and thermal conditions on the operation performance of a solar chimney power generation plant. The authors report that the electrical output was significantly improved when the collector radius was increased from 100 m to 160 m and the divergence angle of the chimney was 1°. The simulation indicated that the performance was improved by increased heat flux, yet power generation was in a saturation state, and the geometry of the chimney had to be optimized to

obtain maximum efficiency [12]. Yoo et al. suggested a filter solar chimney power plant (FSCPP) model for clean air electrical production. According to their report, airflow was reduced by 60% but kept about 95% air cleaning efficiency of the solar cleaning system. Simulation of their research indicated that increasing the height and width of the chimney to 200 m enhanced power output and air filtration efficiency but still experienced electrical production remaining 20-40% of normal SCPP levels under equivalent conditions [13]. Pradhan et al. provided a comprehensive review of performance of solar chimney power plants, hinting at the ability to increase output by as much as threefold by maximizing chimney height, collector area, and turbine design, with the best collector-to-chimney ratios improving efficiency by as much as 30% under controlled conditions. Their review asserted that large-scale SCPPs hold promise as clean energy generators, but commercial-scale implementation is limited by the issue of scalability and cost [14]. Toghraie et al. numerically analyzed the impact of geometric parameters on solar chimney performance using a 3D finite volume approach, revealing that output power and efficiency increased with higher chimney height and collector radius but decreased with greater collector height. The simulations provided optimal chimneys, whose radii were specifically determined to obtain maximum power output and efficiency, and also defined critical design parameters to improve system efficiency for different heat flux [15]. Murena et al. carried out a series of experiments with a 5-meter solar chimney and a 4.5-meter square collector for seven months in Naples. They were able to create a significant correlation between airflow velocity at 2.1 m/s and solar irradiance. In addition, they achieved a good prediction of system performance using their CFD model, which used a temperature field image and simulated airflow currents, hence making optimal design for power performance and purification of air [16]. Mandal et al. analyzed the impact of the divergent angle and the design of the chimney on the performance of solar chimneys-based power plants. According to the findings, the use of a divergent chimney at an angle of +0.75° led to a 47% estimated rise in power generation compared to the traditional design. Further, when optimal chimney angle was combined with ground absorber slope of 0.6°, the power generation was even greater, registering a

phenomenal 80% rise in power generation over the conventional Manzanares plant [17]. Cuce et al. performed a 3D axisymmetric CFD simulation of the Manzanares solar chimney power plant and yielded maximum air velocity as 14.24 m/s at 1000 W/m² solar irradiation—nearly identical to the experimentally measured value of 15.00 m/s—and static pressure went down considerably from the surroundings at the vicinity of the turbine inlet before rising gradually towards the chimney outlet. Output power was also found to be linearly increasing with solar intensity and reducing with rising ambient temperatures from their simulation, with maximum available power being 49,059 W at 293 K atmospheric temperature and 1000 W/m² irradiance [18]. Panda et al. investigated the hybridization of photovoltaic systems and phase-change materials with solar chimney power plants and established that hybrid configurations improved energy efficiency up to 40% and allowed continuous operation even during low light intensity. Their investigation also showed that geometric optimization and heat-recovery schemes improved ventilation performance and water desalination capability, offering a multi-functional solution to sustainable energy and resource management [19]. Pandey et al. adapted a solar chimney design to enable nighttime and low-radiation solar power generation through the integration of a waste heat recovery system, thus achieving a maximum thermal efficiency of 5%, which is a considerable improvement over traditional solar chimney. Computational fluid dynamics (CFD) simulation confirmed that the use of syltherm-800 as a heat transfer fluid and an aluminum alloy heat exchanger plate greatly enhanced airflow and temperature rise, especially with continuous waste heat supply [20]. Padhi et al. performed an examination to study the effect of geometrical modifications in airflow and thermodynamic performance of a solar chimney from the Manzanares prototype. According to their results, they proved that greater height, diameter, or radius of the chimney or collector resulted in higher air velocity with the most favourable results when turbines were mounted at the collector exit and not inside the chimney. Their simulations also proved that a rise in roof height negatively impacted performance, thus highlighting the importance of design adjustments planned for the best solar chimney efficiency [21]. A systematic numerical and ANN-based study demonstrated that adjusting collector inlet height, chimney

diameter, and divergence can increase the output of a solar updraft tower by up to 12 times compared to the classical Manzanares design, offering a reliable methodology for performance enhancement and efficient design [22]. A comprehensive review of solar updraft towers highlights that while design modifications and hybridization improve performance, challenges like low efficiency, large land use, and high initial costs hinder commercialization, urging focused experimental research and scalable hybrid solutions for future deployment [23].

The objective of this research is to investigate the impact of varying key structural dimensions of a solar chimney—such as collector radius, collector height, chimney height, chimney radius, base and top radii, and chimney angle—on the performance of the system. Specifically, the study aims to analyse how these modifications influence critical state variables, including air velocity, temperature, and vacuum pressure at the chimney inlet, with the goal of optimizing the solar chimney's efficiency for enhanced heat transfer, improved airflow, and overall performance. The novelty of this research lies in its holistic approach to solar chimney optimization, where multiple dimensional parameters are varied and their effects on system performance are thoroughly analysed. This study offers new insights into the relationships between collector and chimney dimensions and their influence on air velocity, temperature, and pressure. By simultaneously considering these factors, the research provides a comprehensive understanding of how to optimize solar chimney design while addressing the inherent trade-offs between performance and structural constraints.

2. CAD Model Geometry

The computer aided design (CAD) geometry of a solar chimney as shown in Figure 1 represents the 3D model of its key components, including the collector, chimney shaft, and base dimensions. These elements interact to generate airflow by converting solar energy into thermal energy, creating the pressure difference necessary to drive air upwards. In the Manzanares solar

chimney, the chimney height is 195 meters, crucial for establishing the pressure differential that drives air movement. A taller chimney increases vacuum pressure, enhancing airflow, but must be optimized to maintain air residence time for efficient temperature regulation. The chimney radius is 5 meters, balancing airflow velocity and pressure. A smaller radius boosts velocity but reduces pressure, while a larger radius decreases both. The collector's average roof height is 1.8 meters, influencing the amount of air that can be heated. A higher collector increases air volume, while a lower height improves heat concentration, optimizing the pressure difference. The collector radius is 122 meters, determining the surface area for solar absorption. The geometrical dimensions can be perceived from Table 1. A larger radius increases heat generation and the air volume directed into the chimney, improving system efficiency.

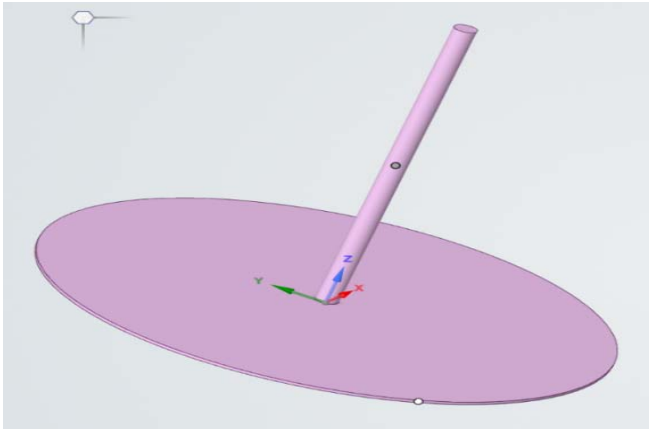

Figure 1. CAD model of solar chimney in Ansys space claim.

Table 1. Geometrical dimensional parameters

Solar chimney height, $H(m)$	195
Solar chimney radius, $R(m)$	5
Collector roof height, $h(m)$	1.8
Collector radius, $r(m)$	122

3. Governing Mathematical Equation

The computer aided design (CAD) geometry of a solar chimney as shown in Figure 1 represents the 3D model of its key components, including the collector, chimney shaft, and base dimensions. These elements interact to generate airflow by converting solar energy into thermal energy, creating the pressure difference necessary to drive air upwards.

Continuity equation:

$$\frac{1}{r}\frac{\partial(r\rho u)}{\partial z}+\frac{\partial(\rho\upsilon)}{\partial z}=0. \tag{1}$$

Navier-Stokes equation:

$$\frac{\partial p}{\partial r}=\frac{\partial}{\partial r}\left[2\mu\frac{\partial u}{\partial r}+\mu'\nabla\cdot\vec{\upsilon}\right]+\frac{\partial}{\partial z}\left[\mu\left(\frac{\partial u}{\partial z}+\frac{\partial\upsilon}{\partial r}\right)\right]+\frac{2\mu}{r}\left(\frac{\partial u}{\partial r}-\frac{\upsilon}{r}\right), \tag{2}$$

$$\frac{\partial p}{\partial r}=\frac{\partial}{\partial r}\left[2\mu\frac{\partial\upsilon}{\partial z}+\mu'\nabla\cdot\vec{\upsilon}\right]+\frac{\partial}{r\partial r}\left[\mu r\left(\frac{\partial u}{\partial z}+\frac{\partial\upsilon}{\partial r}\right)\right]. \tag{3}$$

Energy equation:

$$\left[\frac{1}{r}\frac{\partial}{\partial r}(rTu)+\frac{\partial}{\partial z}(T\upsilon)\right]=\frac{1}{r}\frac{\partial}{\partial r}\left(rw\frac{\partial T}{\partial r}\right)+\frac{\partial}{\partial z}\left(w\frac{\partial T}{\partial z}\right)+\frac{1}{r}\frac{\partial}{\partial r}(rPu)$$
$$+\frac{\partial}{\partial z}(P\upsilon)\phi. \tag{4}$$

Kinetic turbulent energy:

$$\frac{\partial}{\partial t}(\rho\varepsilon)+\frac{\partial}{\partial x}(\rho u\varepsilon)+\frac{\partial}{\partial y}(\rho\upsilon\varepsilon)=\left(\mu+\frac{\mu_t}{\sigma_\varepsilon}\right)\left(\frac{\partial^2}{\partial x^2\varepsilon}+\frac{\partial^2}{\partial y^2}\right)$$
$$+\rho G_k+G_b-\rho\varepsilon. \tag{5}$$

The turbulent Prandtl numbers for ε and k are denoted as σ_ε and σ_k, respectively. The typical value of the model constant (C3) is generally assumed to fall within the range of 0 to 10^{-3}. Experimentally determined values for the turbulent model constants are $C_1=1.44$, $C_2=1.92$, $\sigma_\varepsilon=1.3$ and $\sigma_k=1$.

4. Solution Methods

The CFD analysis was carried out using the Ansys solid-fluid heat transfer module, integrated with the Fluent solver in Discovery 2023 R1. The simulation adopted the finite volume method (FVM) to solve the governing equations. The meshing of solar chimney in Ansys space claim can be referred from Figure 2. A pressure-based solver operating under steady-state conditions with absolute velocity formulation was utilized, with gravitational acceleration set to 9.81 m/s² along the *x*-axis. The *k*-epsilon turbulence model with renormalization group (RNG) modifications was applied, and its second-order differential equations were solved using FVM. To capture near-wall effects accurately, an enhanced wall treatment method accounting for full buoyancy effects was employed. The simulation also incorporated air's physical properties as a function of temperature for improved realism.

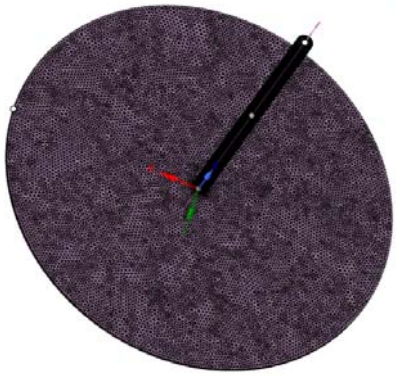

Figure 2. Meshing of solar chimney in Ansys space claim.

The solar radiation was modelled using the discrete ordinates (DO) radiation model, with air assigned zero values for both absorption and scattering coefficients. The thermal coefficient and refractive index of air were set at 0.00331 and 1, respectively. The simulation defined the air inlet as a pressure inlet and the air outlet as a pressure outlet. For the soil-based wall absorber, an absorptivity of 0.89 was applied. The Spanish prototype incorporated multiple materials with distinct properties. The chimney, constructed from concrete, had a density of 2100 kg/m³, thermal conductivity

of 1.4 W/m·K, specific heat capacity of 880 J/kg·K, and absorptivity of 0.6. The collector's top surface was made of glass with a density of 2700 kg/m³, thermal conductivity of 0.78 W/m·K, specific heat capacity of 840 J/kg·K and absorptivity of 0.04. The soil used for the collector's absorber had a density of 1900 kg/m³, thermal conductivity of 1.83 W/m·K, specific heat capacity of 2200 J/kg·K, and absorptivity of 0.8. Glass components were assigned absorptivity and transmissivity values of 0.2 and 0.89, respectively. Additionally, the plate surface had an absorptivity of 0.96, while the concrete chimney wall had an absorptivity of 0.71. These thermophysical properties of solar chimney can be depicted from Table 2. Also, the temperature dependent thermophysical properties of air can be referred from the equations (6) to (9).

The reliability of the numerical model is established by validating the simulated results of the solar chimney with experimental data from the prototype facility in Manzanares, Spain. The air velocity values at different solar flux intensities and times of the day show strong agreement with the experimental observations, with deviations remaining within 8%. The details of this comparison, including the percentage error between the simulated and experimental results, are presented in Table 3. This consistency confirms that the present computational model accurately represents the flow characteristics of the system. A systematic mesh independence study is conducted to achieve an optimal balance between computational cost and solution accuracy. The computational domain is discretized using unstructured tetrahedral elements generated in ANSYS Meshing, and the virtual topology option is applied to handle regions where overlapping of elements occurs. The mesh is refined successively with element counts ranging from approximately 0.083 million to 0.104 million cells. Beyond a mesh size of 0.169 million cells, the variation in updraft velocity remains below 3%, which indicates grid-independent behavior. The final selected mesh exhibits satisfactory orthogonality and skewness values, ensuring numerical accuracy and convergence stability. Both the validation process and the mesh independence study confirm that the numerical approach is robust and that the simulation outcomes can be reliably used for further analysis of solar chimney performance.

Table 2. Thermophysical properties of solar chimney

Thermophysical properties	Absorber (soil)	Glass cover (glass)	Chimney (concrete)
ρ (kg/m^3)	1900	2700	2100
k (W/m-K)	1.83	0.78	1.4
C_p (J/kg-K)	2200	840	880
α (1/m)	0.8	0.04	0.6

Table 3. Validation of CFD results with experimental findings

Solar intensity (W/m²)	Haaf et al. [24, 25]	Present work	Percentage error (%)
200	4.50	4.80	6.67
400	5.30	5.70	7.55
600	6.10	6.70	9.84
800	7.00	7.50	7.14
1000	8.10	8.70	7.41

$$\rho = 345.57(T - 2.6884)^{-1}, \tag{6}$$

$$\begin{aligned} C_p = {} & 1.3864 \times 10^{-13} T^4 - 6.4747 \times 10^{-10} T^2 \\ & + 1.0234 \times 10^{-6} T^2 - 4.3282 \times 10^{-4} T \\ & + 1.3864 \times 10^{-10} + 1.0613, \end{aligned} \tag{7}$$

$$\begin{aligned} k = {} & 1.5797 \times 10^{-17} T^5 + 9.4600 \times 10^{-14} T^4 \\ & - 2.2012 \times 10^{-10} T^2 - 2.3758 \times 10^{-7} T^2 \\ & + 1.7082 \times 10^{-4} T - 7.488 \times 10^{-3}, \end{aligned} \tag{8}$$

$$\begin{aligned} \mu = {} & 2.5914 \times 10^{-15} T^3 - 1.4346 \times 10^{-11} T^2 \\ & + 5.0523 \times 10^{-8} T + 4.1130 \times 10^{-6}. \end{aligned} \tag{9}$$

For numerical methods, the SIMPLE algorithm was utilized for pressure-velocity coupling, with the PRESTO scheme applied for pressure discretization. Spatial gradients were calculated using the least-square cell-based method. A second-order upwind scheme was employed for momentum, turbulent kinetic energy, turbulent dissipation rate, energy, and discrete ordinates equations. Under-relaxation factors for energy and transport equations were maintained at 0.75 to ensure simulation stability.

5. Methods Results and Discussion

This section deals with the discussion of variations in dimensions of solar chimney and its effects on state variables at the chimney inlet. Based on the thermodynamic function's parameters, the performance and hence the optimization of solar chimney can be determined.

5.1. For modification in collector

The analysis presented in Figure 3 demonstrates that as the collector radius expands from 98 m to 122 m, the air velocity and vacuum pressure rise from 21.7 m/s to 25.6 m/s and from -261 Pa to -326 Pa, respectively, alongside an increase in temperature from 54.2°C to 59.9°C. As the collector radius increases, the cross-sectional area for air to be heated and accelerated also grows. This larger area allows for a higher volume of air to be entrained and heated under the solar collector, which increases the buoyancy-driven airflow due to the thermal gradient between the heated air and ambient conditions. With a bigger radius, more solar energy is absorbed, raising the air temperature inside the collector. The increased temperature difference creates stronger buoyancy forces, leading to an increase in air velocity. According to the continuity equation, for a given mass flow rate, the velocity can increase when the pressure drop (vacuum pressure) rises, which is a consequence of enhanced suction effect created by the larger collector. This pressure difference promotes faster airflow through the system. Thus, an expanding collector radius intensifies the thermal and fluid dynamic effects, resulting in higher vacuum pressure, increased air velocity, and elevated air temperature within the solar collector setup.

As shown in Figure 4, increasing the collector height from 1.8 m to 9.2 m results in a reduction in air velocity and temperature, from 26.6 m/s to 22.3 m/s and 56.7°C to 48.7°C, respectively, accompanied by a decrease in vacuum pressure from -355 Pa to -233 Pa. Increasing the collector height enlarges the vertical flow path of the air. A taller collector leads to a longer travel distance, causing more frictional losses and resistance to airflow inside the system. This results in a reduction in the airflow velocity, as friction dissipates kinetic energy. Additionally, a higher collector height increases the

air volume inside, which can dilute the heat concentration from the solar radiation. Thus, the temperature rise of the air is lowered because the same thermal energy is spread over a larger volume of air, reducing the temperature gradient that drives buoyancy. The combined effect of reduced buoyancy forces due to lower temperature and increased flow resistance from a taller structure reduces the vacuum pressure created inside the collector. This weaker pressure difference translates to slower air movement. Hence, increasing collector height causes energy losses due to friction, lowers thermal driving forces, and subsequently reduces air velocity, temperature, and vacuum pressure within the system.

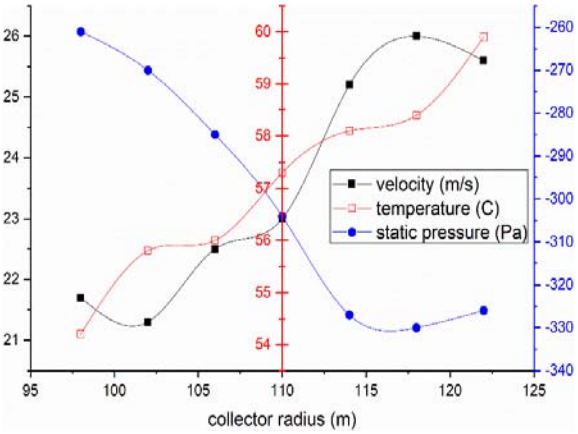

Figure 3. Velocity, temperature, and pressure with collector radius.

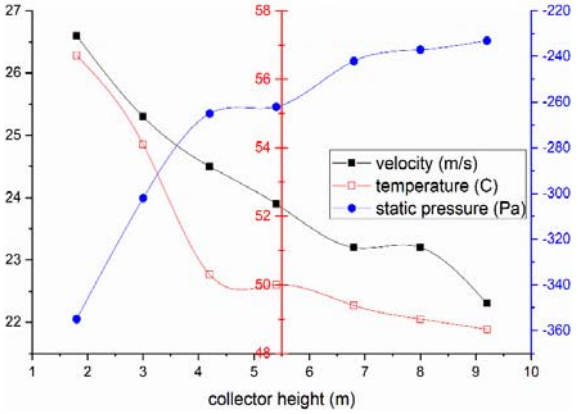

Figure 4. Velocity, temperature, and pressure with collector height.

5.2. For modification in chimney

As illustrated in Figure 5, increasing the chimney height from 115 m to 255 m leads to a rise in air velocity and vacuum pressure, from 21.7 m/s to 27.8 m/s and -218 Pa to -374 Pa, respectively, while the temperature decreases from 57.3°C to 52°C. A taller chimney creates a stronger buoyancy effect because the vertical column of heated air extends over a greater height. This enhances the pressure difference between the bottom and top of the chimney, generating a greater driving force for airflow. Consequently, air velocity increases due to this amplified suction effect. However, as the chimney height grows, the residence time of air within the collector and chimney decreases, meaning air spends less time being heated. This leads to a reduction in the temperature of the air at the chimney outlet, since there is less opportunity for heat gain. Furthermore, the higher velocity caused by increased chimney height results in more efficient air movement, but the temperature drop along the chimney may be more pronounced due to faster convection and heat losses. Together, these phenomena culminate in higher vacuum pressure and airflow but lower air temperatures with increasing chimney height.

As depicted in Figure 6, increasing the chimney radius from 3.5 m to 11 m results in a reduction in air velocity and temperature, from 30.2 m/s to 18 m/s and 84.8°C to 54.2°C, respectively, along with a decrease in vacuum pressure from -440 Pa to -158 Pa. Increasing the chimney radius enlarges the cross-sectional area through which air flows. For a given mass flow rate, a larger flow area reduces the velocity due to the continuity principle, as the same volume of air moves more slowly through a wider space. Moreover, a wider chimney allows for greater air volume inside, but this dilutes the heat energy absorbed by the air. As a result, the air temperature decreases because the solar energy is spread over a larger volume of air, lowering the thermal gradient that drives buoyancy and airflow. The reduction in velocity and temperature also leads to a drop in the pressure difference or vacuum pressure inside the chimney. Lower vacuum pressure reduces the effective suction force that drives air movement, further contributing to lower airflow

speeds. Thus, expanding chimney radius causes a combined effect of reduced air velocity, temperature, and vacuum pressure, primarily governed by the conservation of mass, energy dilution, and weakened buoyant forces in the solar chimney system.

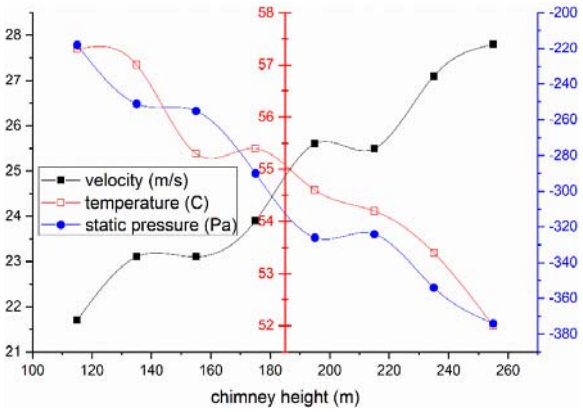

Figure 5. Velocity, temperature, and pressure with chimney height.

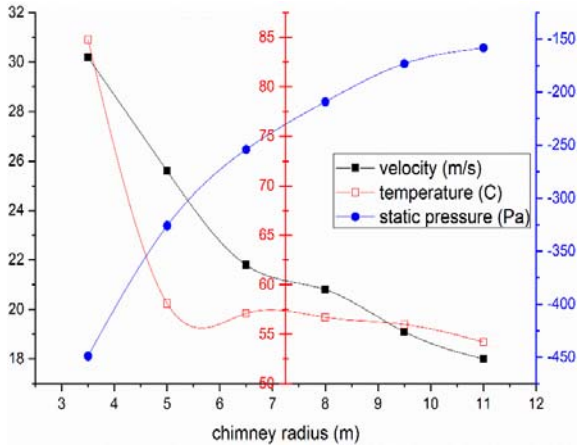

Figure 6. Velocity, temperature, and pressure with chimney radius.

5.3. For modification in base and top

As shown in Figure 7, increasing the bottom radius of the chimney from 4 m to 7 m causes a reduction in air velocity and vacuum pressure, from 29.1 m/s to 18.8 m/s and -402 Pa to -173 Pa, respectively, while the temperature

increases from 54.1°C to 60.9°C. Increasing the bottom radius of the chimney expands the cross-sectional area at the base. For a given volumetric flow rate, this leads to a lower air velocity since the air has more space to move through, as dictated by the continuity principle. The broader base also reduces the pressure drop (or vacuum) within the chimney because the suction force per unit area diminishes with increased area. Despite the reduction in airflow speed, the increase in base area allows for more efficient capture and retention of solar heat at the lower part of the chimney. The larger area exposed to solar energy absorption results in greater localized heating of the air near the base, which can cause the air temperature to rise even though the overall velocity is lower. Therefore, a wider chimney base leads to slower-moving air and diminished vacuum pressure but enables more intense heating near the bottom, raising the air temperature at this location. As illustrated in Figure 8, increasing the top radius of the chimney from 4 m to 7 m leads to an increase in air velocity and temperature, from 20.1 m/s to 30.6 m/s and 55.2°C to 61.5°C, respectively, along with a rise in vacuum pressure from -217 Pa to -427 Pa. Expanding the top radius of the chimney reduces the flow resistance at the exit, making it easier for hot air to escape. This enhances the pressure differential between the base and outlet of the chimney, intensifying the buoyancy-driven flow and resulting in a higher air velocity upward. As the flow restriction is lessened, the hot air can move more rapidly through the chimney. The faster movement reduces stagnation and mixing losses, allowing the retained solar heat within the air column to be better preserved, which elevates the air temperature at the outlet. Additionally, the increased airflow and greater exit area create a larger suction (lower pressure) effect at the base of the chimney. This generates a stronger vacuum pressure, further boosting the driving force for air movement. Overall, these changes—reduced exit resistance, improved ventilation, strengthened buoyancy, and enhanced suction-lead to simultaneous increases in air velocity, temperature, and vacuum pressure when the chimney’s top radius is increased.

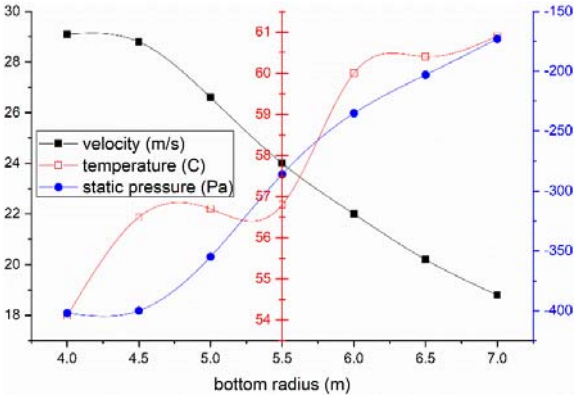

Figure 7. Velocity, temperature, and pressure with bottom radius.

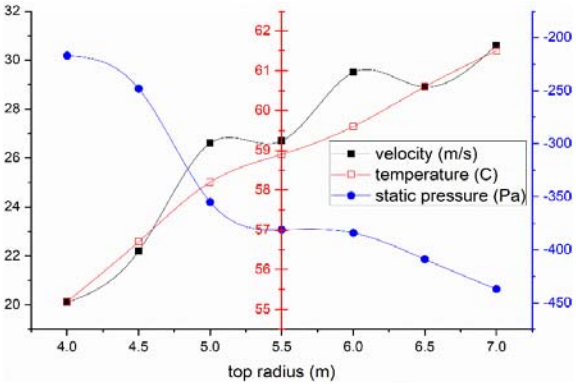

Figure 8. Velocity, temperature, and pressure with top radius.

5.4. For modification in chimney angle (θ°):

As shown in Figure 9, increasing the chimney angle from 0° to 60° toward the horizontal results in a reduction in air velocity and temperature, from 26.6 m/s to 23.7 m/s and 59.7°C to 56.7°C, respectively, along with a decrease in vacuum pressure from -355 Pa to -290 Pa. As the chimney is inclined from vertical toward horizontal, the effective height component in the vertical direction decreases. Since buoyancy-driven flow relies on the vertical column of heated air to generate pressure differences, a lower effective height reduces the gravitational potential difference, weakening the natural draft and thus lowering air velocity. The inclined orientation also increases flow resistance due to longer path length and potential flow

separation or recirculation zones, especially at higher angles. This disrupts smooth convection, dissipates kinetic energy, and further reduces airflow speed. With slower air movement, heat transfer from the collector surface to the air becomes less efficient, and the residence time of air in the heated zone increases, but the overall convective heat gain diminishes due to reduced flow momentum. Additionally, greater exposure to ambient cooling along the extended surface of the inclined chimney enhances thermal losses. The combined effect of reduced buoyancy, increased frictional losses, and greater heat dissipation leads to lower vacuum pressure, decreased air velocity, and reduced temperature as the chimney angle increases toward the horizontal.

The temperature contour of solar chimney can be referred from Figure 10.

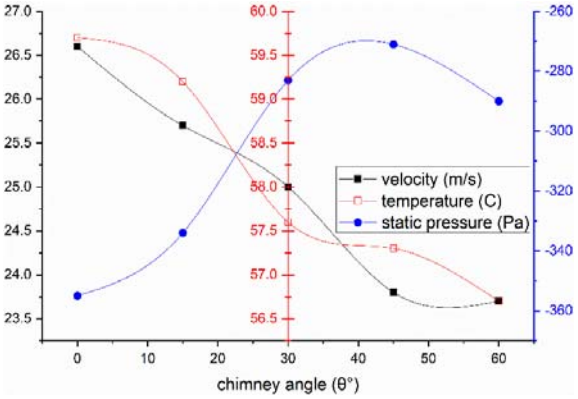

Figure 9. Velocity, temperature, and pressure with chimney angle.

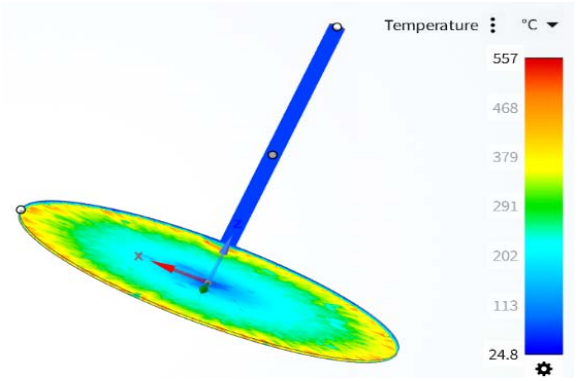

Figure 10. Temperature contour of solar chimney.

6. Conclusion

As the optimization of solar chimney performance depends on adjusting structural parameters to maximize efficiency while ensuring system stability. Increasing the collector radius from 98 m to 122 m results in a 17.9% increase in velocity and a 24.9% rise in vacuum pressure, improving heat transfer and system efficiency. However, expanding the collector height from 1.8 m to 9.2 m decreases velocity by 16.2%, temperature by 14.1%, and pressure by 34.4%, indicating a trade-off between air volume and system performance. For the chimney, increasing height from 115 m to 255 m enhances air velocity by 28%, vacuum pressure by 71.6%, but reduces temperature by 9.4%. Reducing chimney radius from 11 m to 3.5 m improves pressure by 64%, although velocity and temperature decrease significantly. Modifications to the chimney's base and top radii demonstrate that increasing the bottom radius from 4 m to 7 m reduces air velocity by 35.5% but raises temperature by 12.6%, while increasing the top radius enhances both velocity (52.2%) and temperature (11.4%). Changing the chimney angle from 0° to 60° results in a 10.9% decrease in velocity, a 5.0% drop in temperature, and an 18.3% reduction in vacuum pressure. These findings highlight that optimizing these dimensions is crucial for maximizing solar chimney efficiency while maintaining structural stability and performance.

Acknowledgement

The authors thank the anonymous referees for their comments and feedback on earlier version of this document.

References

[1] H. Setayesh, A. Kasaeian, M. Najafi, M. M. Pour and M. Akbari, The effects of geometric factors on power generation performance in solar chimney power plants, Energy 310 (2024), 133264. https://doi.org/10.1016/j.energy.2024.133264.

[2] C. Wang, Y. Wu, C. Hua, X. Zhao, J. Zang and N. Gao, Numerical investigation on the influence of geometric parameters on turbulent flow and thermal performance in the roof solar chimney, Build. Environ. 267 (2025), 112210. https://doi.org/10.1016/j.buildenv.2024.112210.

[3] P. M. Cuce, E. Cuce, D. K. Mandal, D. K. Gayen, M. Asif, A. Bouabidi, S. Alshahrani, C. Prakash and M. E. M. Soudagar, ANN and CFD driven research on main performance characteristics of solar chimney power plants: Impact of chimney and collector angle, Case Stud. Therm. Eng. 60 (2024), 104568. https://doi.org/10.1016/j.csite.2024.104568.

[4] M. J. Saleh, F. S. Atallah, S. Algburi and O. K. Ahmed, Enhancement methods of the performance of a solar chimney power plant: Review, Results Eng. 19 (2023), 101375. https://doi.org/10.1016/j.rineng.2023.101375.

[5] A. Khayyaminejad, S. Jalilian and A. Fartaj, Twisted tapes in solar chimney-earth air heat exchangers for equipment downsizing and passive cooling, J. Build. Eng. 98 (2024), 111128. https://doi.org/10.1016/j.jobe.2024.111128.

[6] M. A. Aziz and A. M. Elsayed, Thermofluid effects of solar chimney geometry on performance parameters, Renew, Energy 200 (2022), 674-693. https://doi.org/10.1016/j.renene.2022.10.022.

[7] T. Singh and A. Kumar, Numerical analysis of the divergent solar chimney power plant with a novel arc and fillet radius at the chimney base region, Renew. Energy 228 (2024), 120504. https://doi.org/10.1016/j.renene.2024.120504.

[8] M. H. H. M. A. Tork, E. Houshfar and M. Ashjaee, Integrating geothermal energy and a solar chimney to maximize renewable energy production: An analytical investigation of a novel hybrid system, Renew. Energy 230 (2024), 120827. https://doi.org/10.1016/j.renene.2024.120827.

[9] O. Ardila, J. Quiroga and C. Amaris, Assessment of solar chimney potential for passive ventilation and thermal comfort in the northeast of Colombia, Results Eng. 20 (2023), 101641. https://doi.org/10.1016/j.rineng.2023.101641.

[10] J. Gong, L.W. Chew and P. S. Lee, Theoretical model for high-rise solar chimneys and optimum shape for uniform flowrate distribution, Energy 298 (2024), 131358. https://doi.org/10.1016/j.energy.2024.131358.

[11] S. Bagheri and M. G. Hassanabad, Numerical and experimental investigation of a novel vertical solar chimney power plant for renewable energy production in urban areas, Sustain, Cities Soc. 96 (2023), 104700. https://doi.org/10.1016/j.scs.2023.104700.

[12] M. R. Torabi, M. Hosseini, O. A. Akbari, H. H. Afrouzi, D. Toghraie, A. Kashani and A. Alizadeh, Investigation of the performance of a solar chimney power plant for improving the efficiency and increasing the outlet power of turbines using computational fluid dynamics, Energy Rep. 7 (2021), 4555-4565. https://doi.org/10.1016/j.egyr.2021.07.044.

[13] S. Yoo, S. Oh and A. A. Hachicha, Numerical simulation and performance evaluation of filter-equipped solar chimney power plants, Appl. Therm. Eng. 218 (2023), 119284. https://doi.org/10.1016/j.applthermaleng.2022.119284.

[14] S. Pradhan, R. Chakraborty, D. K. Mandal, A. Barman and P. Bose, Design and performance analysis of solar chimney power plant (SCPP): A review, Sustain. Energy Technol. Assess. 47 (2021), 101411. https://doi.org/10.1016/j.seta.2021.101411.

[15] D. Toghraie, A. Karami, M. Afrand and A. Karimipour, Effects of geometric parameters on the performance of solar chimney power plants, Energy 162 (2018), 1052-1061. https://doi.org/10.1016/j.energy.2018.08.086.

[16] F. Murena, I. Gaggiano and B. Mele, Fluid dynamic performances of a solar chimney plant: Analysis of experimental data and CFD modelling, Energy 249 (2022), 123702. https://doi.org/10.1016/j.energy.2022.123702.

[17] D. K. Mandal, N. Biswas, N. K. Manna and A. C. Benim, Impact of chimney divergence and sloped absorber on energy efficacy of a solar chimney power plant (SCPP), Ain Shams Eng. J. 15 (2024), 102390. https://doi.org/10.1016/j.asej.2023.102390.

[18] E. Cuce, P. M. Cuce and H. Sen, A thorough performance assessment of solar chimney power plants: Case study for Manzanares, Clean. Eng. Technol. 1 (2020), 100026. https://doi.org/10.1016/j.clet.2020.100026.

[19] T. K. Panda, M. Pandey, A. M. Mohanty, I. Mishra and M. Pandey, Revolutionizing solar chimneys in harvesting clean energy: A review, JP J. Heat Mass Transf. 37(5) (2024), 575-600. https://doi.org/10.17654/0973576324038.

[20] M. Pandey, B. N. Padhi and I. Mishra, Performance analysis of a waste heat recovery solar chimney for nocturnal use, Eng. Sci. Technol. Int. J. 24 (2021), 1-10. https://doi.org/10.1016/j.jestch.2020.11.009.

[21] B. N. Padhi, M. Pandey and I. Mishra, Relation of change in geometrical parameters in the thermal performance of solar chimney, J. Mech. Sci. Technol. 35 (2021), 4737-4746. https://doi.org/10.1007/s12206-021-0939-8.

[22] D. K. Mandal, N. Biswas, N. K. Manna, D. K. Gayen and A. C. Benim, Application of artificial neural network for comparative performance assessment of solar chimney plant for green energy production, Sci. Rep. 14 (2024), 979. https://doi.org/10.1038/s41598-023-46505-1.

[23] N. Biswas, D. K. Mandal, S. Bose, N. K. Manna and A. C. Benim, Experimental Treatment of Solar Chimney Power Plant—A Comprehensive Review, Energies 16 (2023), 6134. https://doi.org/10.3390/en16176134.

[24] W. Haaf, K. Friedrich, G. Mayr and J. Schlaich, Solar chimneys Part I: Principle and construction of the pilot plant in Manzanares, International Journal of Solar Energy 2 (1983), 3-20. https://doi.org/10.1080/01425918308909911.

[25] W. Haaf, Solar chimneys Part II: Preliminary test results from the Manzanares pilot plant, International Journal of Solar Energy 2 (1984), 141-161. https://doi.org/10.1080/01425918408909921.